

X-ray diffraction characterization of microdefects in silicon crystals after high-energy electron irradiation

V. B. Molodkin¹, S. I. Olikhovskii^{*1}, E. G. Len¹, B. V. Sheludchenko¹, S. V. Lizunova¹, Ye. M. Kyslovs'kyy¹, T. P. Vladimirova¹, E. V. Kochelab¹, O. V. Reshetnyk¹, V. V. Dovganyuk², I. M. Fodchuk², T. V. Lytvynchuk², V. P. Klad'ko³, and Z. Świątek⁴

¹G. V. Kurdyumov Institute for Metal Physics of NASU, Vernadsky Blvd. 36, 03680 Kyiv, Ukraine

²Yu. Fed'kovych Chernivtsi National University, Kotsyubynsky Str. 2, 58032 Chernivtsi, Ukraine

³V. Lashkaryov Institute of Semiconductor Physics of NASU, pr. Nauki 45, 03680 Kyiv, Ukraine

⁴Institute of Metallurgy and Materials Science, Polish Academy of Science, 25 Reymonta Str., 30-059 Krakow, Poland

Received 28 November 2010, revised 27 June 2011

Published online 13 October 2011

Keywords electron irradiation, microdefects, silicon, X-ray diffraction

* Corresponding author: e-mail olikhovsky@meta.ua, Phone: +(380) 44 424-10-05, Fax: +(380) 44 424-25-61

The quantitative characterization of complex microdefect structures in silicon crystals grown by Czochralski method and irradiated with various doses of high-energy electrons (18 MeV) has been performed by methods of the high-resolution X-ray diffraction. The concentrations and average sizes of dislocation loops and oxygen precipitates have been

determined by using the combined treatment of reciprocal space maps and rocking curves based on the analytical formulas of the statistical dynamical theory of X-ray diffraction by imperfect crystals with randomly distributed microdefects of several types.

© 2011 WILEY-VCH Verlag GmbH & Co. KGaA, Weinheim

1 Introduction The investigation of changes of the structure and physical properties of silicon and other semiconducting materials under the influence of electron irradiation is of large scientific and technological importance (see, e.g., Refs. [1–5]). Particularly, the obtained knowledge can provide the possibility of aimed influence on structural changes and related mechanical, electro-physical, optical, and other physical properties of the newly developed functional materials.

Experimental investigations of the generation and transformation of defects in semiconductors after an electron irradiation are concerned mainly with intrinsic point defects and their small complexes with impurity atoms. For the observation of these defects different spectroscopic methods are used [3–8]. The small clusters of intrinsic point defects and new phase particles in electron-irradiated semiconductor crystals were observed also by means of transmission electron microscopy [9] and differential X-ray diffractometry [10, 11].

Far less works are devoted to the observation of large growth microdefects in such crystals and analysis of their

interactions with primary radiation defects (see, e.g., [12]). Corresponding investigations can be carried out only by means of high-resolution X-ray diffractometry with the use of results of the statistical dynamical theory of X-ray diffraction in imperfect crystals, which has been developed recently and gives the self-consistent description of coherent and diffuse components of diffraction intensity in crystals with several types of defects of arbitrary sizes [13, 14].

The aim of the present work consists in the determination of changes of the concentrations and sizes of dominant types of microdefects in the silicon single crystals grown by Czochralski method (Cz Si) after their irradiation with high-energy electrons by using methods of the high-resolution X-ray diffractometry.

2 Basic equations

2.1 Reciprocal space maps Differential X-ray diffraction intensity distributions measured by the triple-crystal diffractometer (TCD) from an imperfect crystal with randomly distributed defects are consisted of the sum of coherent (I_B) and diffuse (I_D) components (see Ref. [15] and

references therein). These components depend on the angular deviations $\Delta\theta$ and $\Delta\theta'$ of the crystal under investigation and analyzer crystal, respectively:

$$I(\Delta\theta, \Delta\theta') = I_{\text{coh}}(\Delta\theta, \Delta\theta') + I_{\text{diff}}(\Delta\theta, \Delta\theta'). \quad (1)$$

The coherent component of the two-dimensional intensity distribution measured by TCD can be represented approximately in the case of quasi-dispersionless ($m, -n, m$) geometry as

$$I_{\text{coh}}(\Delta\theta, \Delta\theta') = I_0 \int_{-\infty}^{\infty} R_M(b_M^{-1}[b_S^{-1}(x - \Delta\theta) - \Delta\theta']) \times R_{\text{coh}}(b_S^{-1}(x - \Delta\theta))R_A(x - \Delta\theta')dx, \quad (2)$$

where I_0 is the intensity of incident X-ray beam, R_M and R_A are reflection coefficients of monochromator and analyzer crystal systems, b_M and b_S are asymmetry parameters of monochromator and sample crystals, respectively. The expression for the coherent component of the reflection coefficient $R_{\text{coh}}(\Delta\theta)$ for imperfect crystal containing randomly distributed microdefects has been derived elsewhere earlier [13, 16] and takes into account all the dynamical scattering effects including the extinction of Bragg waves due to the diffuse scattering (DS) on defects.

The diffuse component of the diffraction intensity measured by TCD can be represented by the following expression [15]:

$$I_{\text{diff}}(\Delta\theta, \Delta\theta') = I_0 \int_{-\infty}^{\infty} R_M(x)dx \times \int_{-\infty}^{\infty} r_{\text{diff}}(k_x, k_z)R_A(x' - \Delta\theta')dx'. \quad (3)$$

The function $r_{\text{diff}}(k_x, k_z)$ in Eq. (3) represents the diffuse component $R_D(\mathbf{k})$ of the differential reflection coefficient which is calculated as the square of the dynamical diffuse scattering amplitude, which is averaged over random distribution of defects and integrated over a vertical divergence:

$$r_{\text{diff}}(k_x, k_z) = K^{-1} \int R_D(\mathbf{k})dk_y, \quad (4)$$

where $K = 2\pi/\lambda$, λ is X-ray wavelength. The complex momentum transfer $\mathbf{q} = \mathbf{k} + i\mu_i\mathbf{n}$, which is contained in the expression for R_D in Eq. (4), includes the interference absorption coefficient μ_i . The vector \mathbf{k} describes the deviation from the reciprocal lattice point \mathbf{H} , its components k_x and k_z are lying in the coherent scattering plane (\mathbf{K}, \mathbf{H}), and the component k_z is directed along the normal $\mathbf{n} = \mathbf{e}_z$ to the crystal surface.

When several types (α) of microdefects with size distributions (i) are present in the crystal simultaneously,

Eq. (4) should be simply replaced by the sum of corresponding expressions for each type of defects:

$$r_{\text{diff}}(k_x, k_z) = \sum_{\alpha} \sum_i r_{\text{diff}}^{\alpha i}(k_x, k_z). \quad (5)$$

Similarly, the exponent of static Debye–Waller factor at the absence of correlations between defect positions can be represented as the sum of contributions from each defect population $\{\alpha i\}$:

$$L_{\mathbf{H}} = \sum_{\alpha} \sum_i L_{\mathbf{H}}^{\alpha i}. \quad (6)$$

If the halfwidth of the function r_{diff} in Eq. (4) is significantly larger as compared with halfwidths of the reflection coefficients R_M and R_A , what normally takes place, then these coefficients can be replaced by δ -functions, and Eq. (4) takes the form:

$$I_{\text{diff}}(\Delta\theta, \Delta\theta') \approx I_0 R_{iM} R_{iA} r_{\text{diff}}(k_x, k_z), \quad (7)$$

where R_{iM} and R_{iA} are the integrated reflectivities of monochromator and analyzer crystal systems, respectively. Additionally, it should be remarked that in the case of several defect types with widely ranged defect sizes just the DS intensity distributions from large defects, which give rise to relatively narrow and high peaks, will be the most reliably resolved ones in TCD maps (Figs. 1 and 2).

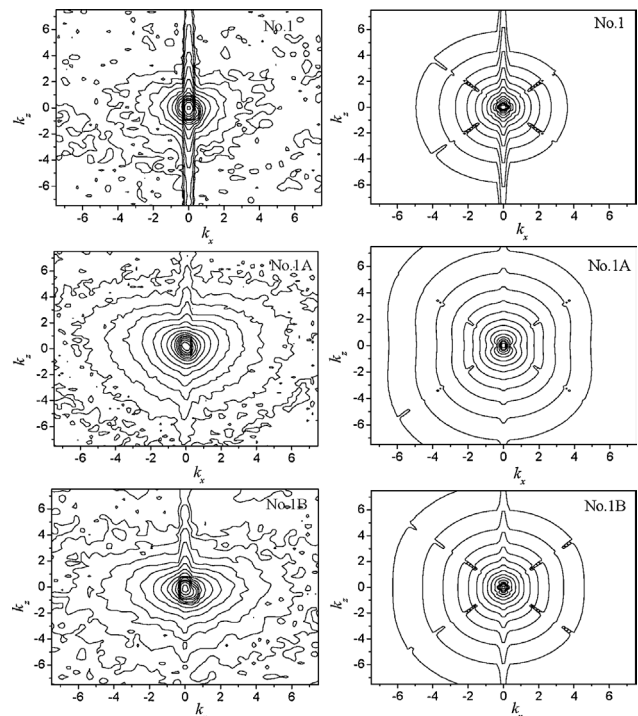


Figure 1 Measured (left) and calculated (right) reciprocal space maps of the as-grown (No. 1) and electron-irradiated (No. 1A and 1B) Cz Si samples, 333 reflection, $\text{CuK}\alpha_1$ radiation (k_x and k_z are measured in $\text{rlu} \times 10^{-4}$).

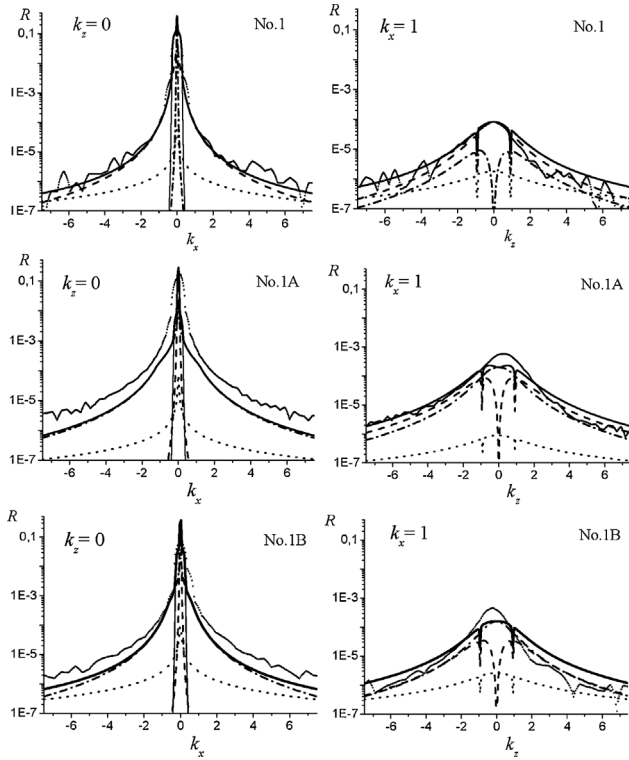


Figure 2 Transversal (left) and longitudinal (right) cross-sections of reciprocal space maps measured by TCD (see Fig. 1). Measured and calculated profiles are shown by markers and thick solid line, respectively, the latter ones consisted of coherent component and DS contributions from large and small dislocation loops, and spherical oxygen precipitates (thin solid, dash-dotted, dotted, and dashed lines, respectively).

2.2 Diffraction profile at ω - 2θ scanning mode

When TCD measurements are carried out in ω - 2θ scanning mode, which is used to eliminate the “pure” coherent scattering intensity component, one should substitute $\Delta\theta' = (1 + b_s^{-1})\Delta\theta$ in both Eqs. (2) and (3). The measured diffraction profile after being normalized to the incidence intensity on the sample crystal can be described in symmetric diffraction conditions ($b_s = b_M = 1$) for unpolarized radiation as

$$R_{\text{TCD}}(\Delta\theta) = \sum_j \int_{-\infty}^{\infty} \left[\rho R_M^{(j)}(x' - 2\Delta\theta) R_{\text{coh}}^{(j)}(x' - \Delta\theta) + \rho_j r_{\text{diff}}^{(j)}(k_x, k_z) \right] R_A^{(j)}(x' - 2\Delta\theta) dx', \quad (8)$$

where the summation is carried out over two polarization states and the notation was used:

$$\rho = 1 / \left(R_{\text{iTCD}}^{(\sigma)} + R_{\text{iTCD}}^{(\pi)} \right), \quad \rho_j = R_{\text{iTCD}}^{(j)} / \left(R_{\text{iTCD}}^{(\sigma)} + R_{\text{iTCD}}^{(\pi)} \right),$$

$$R_{\text{iTCD}} = \int_{-\infty}^{\infty} R_M(x) R_A(x) dx. \quad (9)$$

The integration of the DS intensity component over exit angles in Eq. (8) should be retained to provide smoothing the extinction effects observed on the diffraction profile within the total reflection range. As can be seen from Eq. (8), the diffraction profile measured in ω - 2θ scanning mode still includes the diffuse component which, however, is strongly suppressed due to small factor ρ_j as compared with ρ . It is important to emphasize here that, nevertheless, the DS effects can appear in the coherent component because of the absorption of coherently scattered waves due to a strong DS (see Fig. 2).

2.3 Rocking curve Measurements by TCD in ω -scanning mode without analyzer crystal give the differential reflectivity of the sample under investigation, which is integrated over Ewald sphere, i.e., the rocking curve (RC). The diffuse component of this RC in the case of Bragg diffraction geometry can be written in the approximation of semi-infinite crystal as [16]:

$$R_{\text{diff}}(\Delta\theta) \approx F_{\text{dyn}}(\Delta\theta) \mu_{\text{HH}}(\Delta\theta) / (2\gamma_0 \mu_i). \quad (10)$$

Here, the factor $F_{\text{dyn}} \sim 1$ describes the angular modulation of DS intensity, which is caused by the dynamical interference of strong Bragg waves. The interference absorption coefficient μ_i describes the extinction effect for DS waves and can be estimated as $\mu_i \sim \pi/\Lambda$ within the total reflection range and $\mu_i \approx (1 + b)\mu_0/(2\gamma_0)$ outside (γ_0 is the direction cosine of the incidence wave vector).

The dispersion correction due to DS μ_{HH} in Eq. (10) is the sum of coefficients of the absorption due to DS for defects of α type with i th size $\mu_{\text{ds}}^{\alpha i}$:

$$\mu_{\text{HH}}(\Delta\theta) = \mu_{\text{ds}}(k_0) = \sum_{\alpha} \sum_i \mu_{\text{ds}}^{\alpha i}(k_0), \quad (11)$$

where $k_0 = K\Delta\theta \sin(2\theta_B)$, θ_B is the Bragg angle. The expressions (10) and (11) provide the description of DS intensity contributions from several defect types to the measured diffraction profiles and the absorption of coherent scattering component due to DS, respectively (see Fig. 3).

3 Experimental The investigated silicon samples with (111) surface orientation and almost equal thicknesses ($t \approx 4.26$ mm) were cut from an ingot grown by Czochralski method with (111) growth axis. Two samples have been irradiated with doses 1.8 and 3.6 kGray of high-energy electrons (18 MeV) (No. 1A and 1B, respectively). The as-grown sample No. 1 was used as an etalon for the comparison with the irradiated samples. The irradiation with high-energy electrons was carried out in the Institute of electronic physics (Uzhhorod, Ukraine).

Reciprocal space maps of the samples under investigation were measured by PANalytical X'Pert Pro MRD XL diffractometer for the symmetrical Si (333) reflection of characteristic $\text{CuK}\alpha_1$ radiation. Additionally, the RCs were measured for Si (333) reflection in ω -scanning mode of TCD without using analyzer crystal.

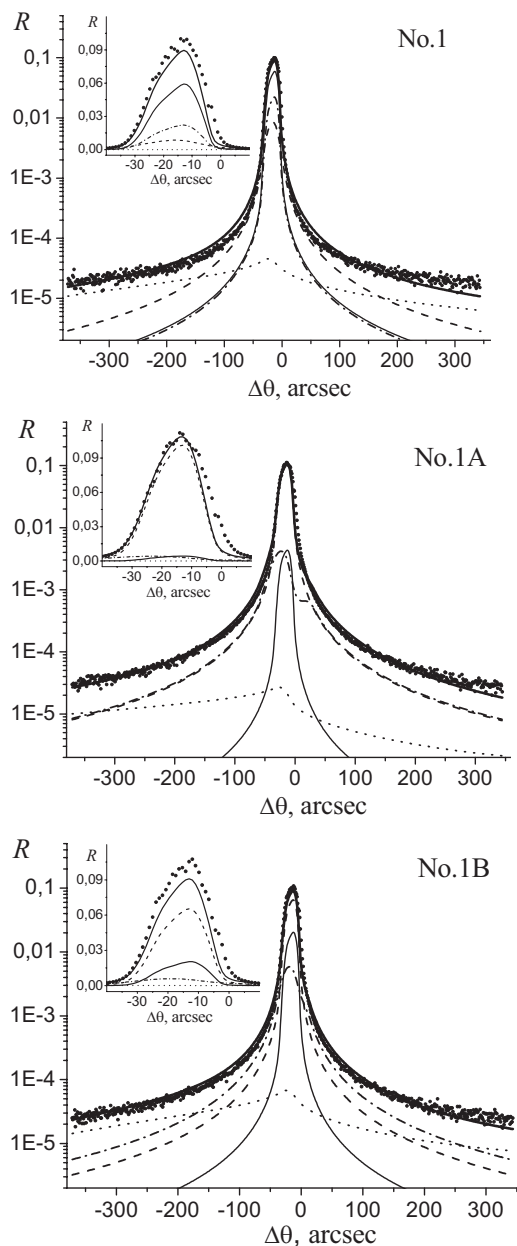


Figure 3 Measured and calculated rocking curves (markers and thick solid line, respectively) for the as-grown (No. 1) and electron-irradiated (No. 1A and 1B) Cz Si samples, 333 reflection, CuK α_1 radiation. The lines are same as in Fig. 2. Inserts show central parts of RCs.

4 Treatment of diffraction patterns and discussion At the analysis of the measured diffraction profiles and reciprocal space maps, the contribution of the thermal DS was neglected as being small in the considered reciprocal space region [16]. The influence of the instrumental function was taken into account only at the treatment of RCs.

The approximate account for instrumental factors at the treatment of maps and their cross-sections has caused the

discrepancies between theory and experiment along a sample streak as well as extinction gaps on the calculated maps along the directions in a reciprocal space, where the Bragg condition is satisfied for wave vectors of incident and scattered DS waves (see Figs. 1 and 2). On the other hand, due to this simplification a significant reduction of the calculation time consumption has been achieved.

For the characterization of the fit quality of RCs, the ordinary and weighted reliability factors were used:

$$R = \sum_j |R_j^{\text{calc}} - R_j^{\text{meas}}| / \sum_j R_j^{\text{meas}},$$

$$R_w = (N + p)^{-1} \sum_j |R_j^{\text{calc}} - R_j^{\text{meas}}| / R_j^{\text{meas}}, \quad j = \overline{1, N}.$$

Here R_j^{meas} and R_j^{calc} are the measured and calculated reflectivities at angular positions $\Delta\theta_j$ of the sample, respectively, N and p are numbers of measurement points and fit parameters, respectively. The R and R_w factors are used to give the estimate of the fit quality in the total reflection range and the uniform estimate within the whole measurement range, respectively.

To perform the detailed quantitative characterization of microdefects in the investigated Cz Si crystals, one should choose an appropriate model of defect structure. Generally, it can be supposed that in both as-grown and electron-irradiated Cz Si crystals two types of microdefects are present simultaneously, namely, oxygen precipitates and interstitial dislocation loops, both randomly distributed without mutual correlation [17].

One of the main problems in the X-ray diffraction characterization of such complicated defect structures occurred in the samples under investigation is that it is difficult to distinguish between the two types of microdefects which have similar (Coulomb-type) asymptotic static displacement fields and cause similar diffraction patterns.

This problem is more strongly exhibited when the DS intensity distribution is integrated over Ewald sphere and thus fine distinct features of the distributions from clusters and dislocation loops are smoothed. Just such a case takes place when RCs are measured by TCD without using analyzer crystal. Particularly, in our consideration it was possible to fit measured RCs with a nearly equal good quality by using only oxygen precipitates of two sufficiently different radii or only dislocation loops of two radii as well.

For this reason, the crucial role of the measured reciprocal space maps consists in the unambiguous ascertainment of the dominant type of microdefects giving a main contribution to the measured differential DS intensity distributions and the determination of approximate estimations of defect characteristics.

Indeed, as can be seen from Fig. 1, for both as-grown (No. 1) and electron-irradiated (No. 1A and 1B) Cz Si samples the form of equal intensity contours on the maps is that characteristic for circular dislocation loops with Burgers vector orientations $\langle 111 \rangle$ (cf. [15]). Their radii R_L have been

Table 1 Characteristics of dislocation loops (radius R_L and number density n_L) and oxygen precipitates (R_P , n_P) in as-grown (No. 1) and electron-irradiated (No. 1A and 1B) Cz Si samples.

sample	dislocation loops		oxygen precipitates		R (%)	R_w (%)
	R_L (μm)	n_L (cm^{-3})	R_P (μm)	n_P (cm^{-3})		
No. 1	0.002 0.12	1×10^{16} 7×10^{11}	1	5×10^6	17	21
No. 1A	0.003 0.07	5×10^{15} 6×10^{12}	1	5×10^7	13	14
No. 1B	0.003 0.07	5×10^{15} 4×10^{12}	1	2×10^7	20	16

estimated by using the measured reciprocal space maps and their cross-sections (Figs. 1 and 2) as being equal to nearly $0.1 \mu\text{m}$ for all the samples. The number densities n_L of dislocation loops in electron-irradiated samples, however, have appeared significantly (nearly by one order of magnitude) larger in comparison with that in as-grown sample (see Table 1).

Simultaneously, the similar increase has been determined for the number density n_P of spherical oxygen precipitates with radii $R_P \approx 1 \mu\text{m}$, which have been added into the consideration to approach the measured diffraction intensities within the total reflection range for both maps and RCs (see Figs. 1–3). It is important here to remark that such improvement of the fit quality was impossible with using any additional dislocation loops of appropriate larger radii because the necessary concentration increase caused the decrease of their Debye–Waller factors which suppressed the corresponding DS intensity contributions.

It should be emphasized that the fitting of the measured reciprocal space maps and their cross-sections was carried out in the mutual consistency with the fit of RCs, i.e., the combined treatment of maps and RCs was performed. The RCs, due to the integration of DS intensity over Ewald sphere, provide a higher sensitivity to small defects as compared with the maps where they are quite invisible.

Particularly, in our consideration the small dislocation loops with radii of few nanometers give the significant contributions at far tails of RCs for all the investigated samples, whereas in TCD diffraction profiles their contributions are negligible (cf. Figs. 2 and 3). Thus, it should be emphasized the exclusively important role of the joint treatment of reciprocal space maps and RCs in the reliable determination of detailed quantitative characteristics of microdefects with a wide spread of sizes.

At the high-energy electron irradiation, two factors influence the transformation of the defect structure in crystal bulk. The first is the creation of radiation defects, in the first place, silicon interstitials and vacancies. The second is an increase of crystal temperature. As can be seen from the obtained characterization results (Table 1), these factors have caused the significant changes of defect characteristics in both irradiated silicon samples as compared with as-grown sample.

Due to the enhanced mobility of dissolved oxygen atoms, the further decomposition of supersaturated solid solution of oxygen in silicon occurs. As consequence, the concentrations of oxygen precipitates in both irradiated silicon samples have raised nearly by an order of magnitude. At the same time, the significant redistribution of sizes and concentrations of small and large dislocation loops takes place because of their interaction with radiation defects and interstitial silicon atoms emitted by growing oxygen precipitates.

Thus, the performed research demonstrates the possibility of using the high-resolution X-ray diffraction methods, additionally to the conventional spectroscopic methods, for studying the defect structure transformations in silicon single crystals under high-energy electron irradiation.

5 Conclusions The obtained characterization results demonstrate the possibility of quantitative diagnostics of the defect structure in high-energy electron irradiated silicon single crystals by combined treatment of high-resolution X-ray diffraction measurements with using the analytical formulas of statistical dynamical theory of X-ray diffraction in imperfect crystals.

The quantitative information on interactions of point defects with microdefects can provide the more correct analysis of the influence of high-energy electron irradiation on the imperfections of silicon single crystals and other semiconductor structures. Particularly, the role of growth microdefects in the transformation of primary and secondary irradiation defects can be elucidated in such investigations.

Acknowledgements This work was performed with financial support of the National Academy of Sciences of Ukraine (Contract No. 3.6.3.13-7/10-D).

References

- [1] M. Mikelsen, E. V. Monakhov, G. Alfieri, B. S. Avset, and B. G. Svensson, *Phys. Rev. B* **72**, 195207 (2005).
- [2] N. Inoue, H. Ohyama, Y. Goto, and T. Sugiyama, *Physica B* **401/402**, 477 (2007).
- [3] A. Khan, J. Gou, M. Imazumi, and M. Yamaguchi, *Appl. Phys. Lett.* **91**, 043503 (2007).

- [4] M. D'Amico, F. Messina, M. Cannas, M. Leone, and R. Boscaino, *Phys. Rev. B* **79**, 064203 (2009).
- [5] F. Tuomisto, V. Ranki, D. C. Look, and G. C. Farlow, *Phys. Rev. B* **76**, 165207 (2007).
- [6] V. Neimash, M. Kras'ko, A. Kraitichinskii, V. Voytovych, V. Tishchenko, E. Simoen, J. M. Rafi, C. Claeys, J. Versluys, O. De Gryse, and P. Clauws, *Phys. Status Solidi A* **201**, 509 (2004).
- [7] A. Nakanishi, M. Suezawa, and N. Fukata, *Jpn. J. Appl. Phys.* **41**, 3629 (2002).
- [8] S. Kaschieva, K. G. Stefanov, and D. Karpuzov, *Appl. Phys. A* **66**, 561 (1998).
- [9] L. Fedina, A. Gutakovskii, A. Aseev, J. Van Landuyt, and J. Vanhellefont, *Phys. Status Solidi A* **171**, 147 (1999).
- [10] K. Karsten and P. Ehrhart, *Phys. Rev. B* **51**, 10508 (1995).
- [11] A. Pillukat, K. Karsten, and P. Ehrhart, *Phys. Rev. B* **53**, 7823 (1996).
- [12] I. M. Fodchuk, T. P. Vladimirova, V. V. Dovganyuk, O. V. Reshetnyk, V. P. Klad'ko, V. B. Molodkin, S. I. Olikhovskii, E. N. Kislovskii, E. V. Kochelab, T. V. Lytvynchuk, and R. F. Seredenko, *Metallofiz. Noveishie Tekhnol.* **32**, 1213 (2010).
- [13] V. B. Molodkin, S. I. Olikhovskii, E. N. Kislovskii, E. G. Len', and E. V. Pervak, *Phys. Status Solidi B* **227**, 429 (2001).
- [14] S. I. Olikhovskii, V. B. Molodkin, E. N. Kislovskii, E. G. Len', and E. V. Pervak, *Phys. Status Solidi B* **231**, 199 (2002).
- [15] V. B. Molodkin, S. I. Olikhovskii, E. G. Len', E. N. Kislovskii, V. P. Klad'ko, O. V. Reshetnyk, T. P. Vladimirova, and B. V. Sheludchenko, *Phys. Status Solidi A* **206**, 1761 (2009).
- [16] V. B. Molodkin, S. I. Olikhovskii, E. N. Kislovskii, T. P. Vladimirova, E. S. Skakunova, R. F. Seredenko, and B. V. Sheludchenko, *Phys. Rev. B* **78**, 224109 (2008).
- [17] A. Borghesi, B. Pivac, A. Sassella, and A. Stella, *J. Appl. Phys.* **77**, 4169 (1995).